Int. J. Heat Mass Transfer. Vol. 27, No. 7, pp. 1039–1054, 1984
Printed in Great Britain

0017–9310/84 $3.00 + 0.00

EFFECT OF INLET, EXIT, AND FIN GEOMETRY ON PIN FINS SITUATED IN A TURNING FLOW

E. M. SPARROW, A. P. SUOPYS and M. A. ANSARI
Department of Mechanical Engineering, University of Minnesota, Minneapolis, MN 55455, U.S.A.

(*Received* 10 *August* 1983 *and in revised form* 7 *October* 1983)

Abstract—Consideration is given to arrays of cylindrical pin fins, with air entering the array at the plane of the fin tips, turning as it passes through the array, and exiting the array in crossflow. Per-fin heat transfer coefficients and overall pressure drops were determined experimentally. A computational model was formulated for determining the array heat transfer rates, with account being taken of the fact that the same rate of airflow does not wash over all of the fins in the array. The model was employed as a basis for comparing the heat transfer rates for various arrays operating at equal pumping power and equal baseplate to inlet-air temperature difference. The special foci of the work were to investigate the effects of various fluid inlet and exit geometries and also to utilize more closely spaced fins than in the past. It was demonstrated that partial shrouding of the inlet could give rise to nearly uniform per-fin heat transfer coefficients throughout the array. Modifications of the exit geometry affected only the less tightly packed arrays and then only at the outermost row of fins.

NOMENCLATURE

A	fin surface area
$\hat{A}$	free-flow area at inlet
$\hat{A}_{\mathrm{I}} \rightarrow \hat{A}_{\mathrm{III}}$	zonal free-flow areas at inlet
c_p	specific heat
D	diameter of pin fin
$\mathscr{D}$	naphthalene–air diffusion coefficient
H	height of fin
h_j	heat transfer coefficient at fin j
$h_{\mathrm{I}} \rightarrow h_{\mathrm{III}}$	zonal heat transfer coefficients, equation (12)
K	per-fin mass transfer coefficient, equation (2)
K_p	pressure loss coefficient, equation (6)
k_f	thermal conductivity of fin
L	side dimension of unmodified inlet opening and baseplate
L_1	side dimension of more-shrouded inlet opening
L_2	side dimension of less-shrouded inlet opening
L_3	side dimension of extended baseplate
$\dot{m}$	mass transfer per unit time and area
m_j	fin efficiency group, equation (11)
Nu	Nusselt number
P	pumping power, $\dot{V}\Delta p$
Δp	array pressure drop
Q	array heat transfer rate
Q_j	heat transfer rate at fin j
$Q_{\mathrm{I}} \rightarrow Q_{\mathrm{III}}$	zonal heat transfer rates
Re	Reynolds number, equation (5)
S	interfin center-to-center distance
Sc	Schmidt number
Sh	per-fin Sherwood number, equation (2)
T_{b}	bulk temperature
$T_{\mathrm{bI}} \rightarrow T_{\mathrm{bIII}}$	zonal bulk temperatures
T_{w}	fin base temperature ($\eta \neq 1$) or fin temperature ($\eta = 1$)
V	reference velocity, equation (4)
$\dot{V}$	volume flow rate, $\dot{w}/\rho$
$\dot{w}$	rate of airflow through array
$\dot{w}_{\mathrm{I}} \rightarrow \dot{w}_{\mathrm{III}}$	zonal airflow rates, equation (13).

Greek symbols

η	fin efficiency
μ	viscosity
ν	kinematic viscosity
ρ	density
ρ_{nw}	naphthalene vapor density at fin surface
ρ_{nb}	naphthalene vapor density in bulk flow.

Subscripts

a	average
e	exit
i	inlet
j	at fin j
I	zone I
II	zone II
III	zone III.

INTRODUCTION

THIS paper describes the second and final portion of a two-part study of a novel pin-fin configuration. The geometrical features of the fin configuration and the directions of fluid flow are illustrated in a pictorial view in Fig. 1 and in a side view in Fig. 2(a). As shown in these figures, an array of rod-like pin fins is situated in an approach flow which enters the array at the plane of the fin tips. The entering fluid at first penetrates the array as a longitudinal flow (i.e. parallel to the axes of the fins). However, owing to the blocking action of the baseplate to which the fins are attached, the fluid is forced to turn and flow toward the outer edges of the array. It passes through the spaces between the edge-adjacent fins and exits the array.

The aforementioned pattern of fluid flow is distinctly different from that for conventional pin-fin arrays.

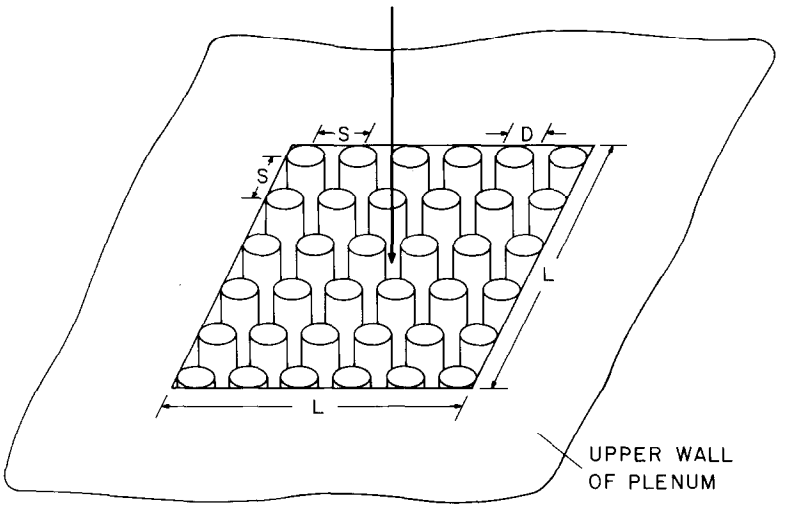

FIG. 1. Pictorial view of the inlet of the pin-fin array.

There, the fluid passes through the array in crossflow to the fins and parallel to the baseplate.

In the first part of this study, refs. [1, 2], per-fin heat transfer coefficients were determined experimentally for the array configuration depicted in Figs. 1 and 2(a). During the course of those experiments, the geometrical parameters S/D and H/D were varied over the respective ranges 2–4 and 4–12, and for each array geometry, the Reynolds number range spanned an order of magnitude. The heat transfer results were correlated and were also employed, along with measured pressure drop information, as input to a performance analysis which compared the various investigated geometries on the basis of equal pumping power. That analysis indicated that better performance (i.e. greater heat transfer at fixed pumping power) could be achieved at larger values of H/D and smaller values of S/D than those that had been investigated.

It was also found that the per-fin heat transfer coefficients at the edge-adjacent fins were higher than those in the central portion of the array. Of particular note is the fact that the cases showing the best performance (on an equal pumping power basis) were those where the aforementioned nonuniformity was least.

The work reported here is results-oriented and has five distinct but interrelated foci. Two of these are concerned with the inlet and exit geometries of the array. The inlet configuration employed in the original experiments [1] was characterized by a square opening whose area is exactly equal to the inlet cross section of the array (e.g. Fig. 1). Here, inlet openings will be employed which are smaller than the array inlet cross section, as illustrated in Fig. 2(b).

As indicated in the diagram, a thin frame-like plate (the inlet shroud) is used to block the edge-adjacent portion of the inlet opening. Such a blockage serves to divert the incoming air from the edge-adjacent fins to those in the interior of the array, with an expected tendency to increase the interior-fin heat transfer coefficients and make them more equal to those in the edge-adjacent region. This expectation was one of the motivations for altering the inlet geometry. Another motivation was the concern that, in practice, the duct used to deliver the air to the array might have a cross section smaller than the inlet cross section of the array. Two different inlet shrouds were employed in the experiments.

In the original experiments, the simplest type of array exit configuration was employed whereby the outboard edges of the outermost set of fins were flush with the

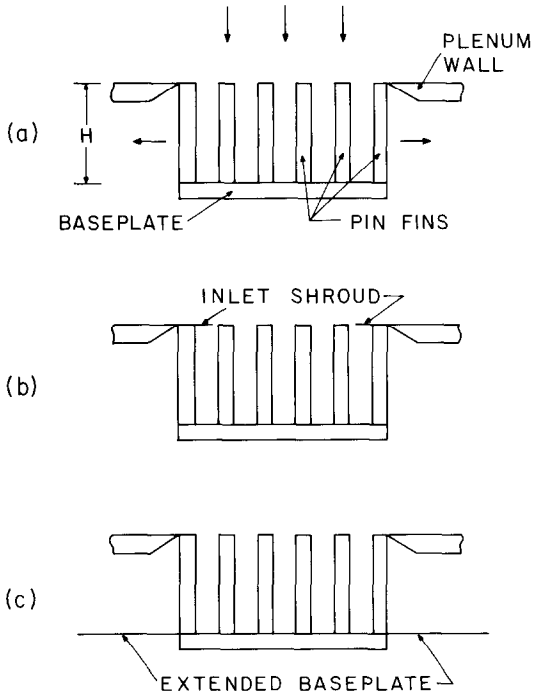

FIG. 2. Side views of the pin-fin array: (a) unmodified array, (b) array with partially shrouded inlet, and (c) array with extended baseplate.

edges of the baseplate (Fig. 1, upper diagram). To investigate the response of the fin heat transfer coefficients to a distinctly different exit configuration, experiments were performed with an extended baseplate as shown in Fig. 2(c).

The third geometry-related focus of the research was a set of experiments for an S/D ratio smaller than the $S/D = 2$ case of the original experiments. As mentioned earlier, an analysis had suggested that improvements in performance could be achieved by operating at smaller S/D. For practical reasons (to be elaborated later), the smallest S/D that could be achieved was 1.48 (nominally 1.5), and experiments were performed for that case.

Although the aforementioned performance analysis had suggested improved heat transfer when $H/D > 12$ (the tallest fins of the original experiments were $H/D = 12$ fins), corresponding experiments were not performed. This is because such relatively tall fins were not deemed to be practical. Also, the performance analysis was approximate in that account had not been taken of departures of the fin efficiency from unity.

For each of the arrays for which heat transfer coefficients are determined here, measurements are also made of the pressure drop across the array.

In addition to the experimental parts of the work, an analytical modeling effort was undertaken to enable the measured per-fin heat transfer coefficients to be applied in practice. The need for the modeling is underscored by the unique nature of the fluid flow throughout the array. In particular, the same mass flow of air does not wash over all the elements of the array. As a consequence, the distribution of the bulk temperature throughout the array cannot be determined by straightforward application of the first law of thermodynamics, as in a conventional duct flow. A model for determining the bulk temperature distribution and the overall heat transfer from the array will be set forth here. The model also takes account of non-unity values of fin efficiency.

The final part of the work is a performance analysis which establishes the ranking of the new geometries for which experiments are performed. The ranking parameter is the rate of heat transfer at fixed pumping power. A key feature of the performance analysis is the use of the new model for the array heat transfer computation.

THE EXPERIMENTS

For determining the per-fin Nusselt numbers, it was found highly advantageous to employ the analogy between heat and mass transfer and to make mass transfer measurements by means of the naphthalene sublimation technique. Those measurements yield the per-fin Sherwood number Sh. As demonstrated in ref. [1], these Sherwood numbers can be transformed to Nusselt numbers for heat transfer in air via the relation

$$Nu = 0.632Sh. \quad (1)$$

In view of the one-to-one correspondence of Sherwood and Nusselt numbers, the phrases mass transfer and heat transfer will be used interchangeably throughout the paper.

Apparatus overview

The general features of the experimental apparatus will now be described. In addition to the pin-fin array, the other major component of the apparatus was a plenum chamber which served to provide the fluid flow environment for the experiments. The plenum was a large rectangular tank, totally sealed except for a square inlet aperture centered in its upper wall and a circular exit port centered in its lower wall. A portion of the upper wall and the square aperture are shown in Fig. 1. Figure 2 shows how the wall was beveled adjacent to the inlet opening. The pin-fin array was situated within the plenum chamber, and its baseplate was supported from the underside in such a way as not to impede the fluid flow.

The exit port of the plenum was coupled to an air-handling system which operated in the suction mode. When this system was activated, air from the laboratory was drawn into and through the fin array as shown in Figs. 1 and 2(a). Upon exiting the array, the air streamed toward the bottom of the plenum where it was collected by the exit port. The air-handling system discharged the naphthalene-laden air outside the laboratory. This arrangement ensured that the air drawn from the laboratory into the fin array was free of naphthalene vapor.

All of the arrays investigated here were made up of 36 fins deployed on square centers on a square baseplate (baseplate side dimension $L = 7.684$ cm, 3.025 in.). The baseplate is shown in Fig. 2(a), where it is seen that the outboard edges of the outermost fins are flush with the edges of the baseplate (the extended baseplates will be described shortly). Arrays having three different S/D ratios were employed—$S/D = 1.48$, 2.22, and 4.10 (nominal values of 1.5, 2, and 4). Different baseplates of identical size were used for the different S/D. The significant geometrical differences among the different S/D arrays can be seen in the upper part of Fig. 3, where the edge-adjacent fins are illustrated.

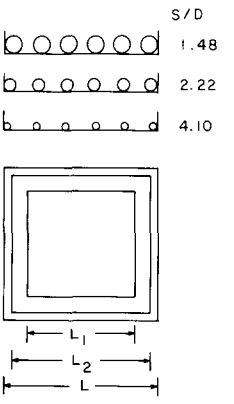

FIG. 3. Layouts of the various arrays and inlet openings.

For each S/D, experiments were performed with dimensionless fin heights H/D of 4 and 12. These heights are believed to typify the practical range.

Two types of pin fins were employed in the experiments. For each array geometry, the two fin types were of identical dimensions (i.e. identical diameter and length). One type was a composite consisting of a coating of naphthalene on a metallic core, while the other type was a metallic cylinder (without naphthalene). Both types of fins were made of drill rod. The purely metallic fins were fabricated by cutting appropriate lengths of rod, machining a shank at one end of each length (to mate with a hole in the baseplate), and squaring off the other end. Owing to the close tolerances of drill rod, no machining of the cylindrical surface was needed.

For the naphthalene-coated fins, the metallic core was fabricated by undercutting both the diameter and length relative to the desired finished dimensions. A screw thread was machined into the cylindrical surface to provide cavities to aid the adhesion of the naphthalene.

The coating was accomplished in a two-step process. In the first step, the core was dipped into a container of molten naphthalene, the dipping being performed in several stages to avoid remelting the naphthalene that had already solidified. During the dipping, the shank end of the core was protected by a Teflon cap to keep it free of naphthalene. Once a sufficiently thick coating had been built up, the coated core was inserted into a lathe and machined until the proper length and diameter dimensions were obtained.

During any given data run, only one of the fins in the array was naphthalene-coated, while all the others were metallic. Thus, only one fin participated directly in the mass transfer process. The procedure of employing a single transferring element situated in a multi-element array is quite common in the testing of tube-bank-type heat exchangers. It was adopted here because of the great simplifications that it afforded in the execution of the experiments.

The location of the naphthalene-coated fin was varied from run to run in order to obtain per-fin mass transfer coefficients at all the fin locations in the array. Although there are 36 fins in the array, it was not necessary to collect data at each fin location. Because of the geometrical symmetries inherent in the array, only six different measurement sites had to be employed to collect information sufficient for the entire array. These symmetries can be visualized in Fig. 1, where the array is seen to naturally subdivide itself into four identical quadrants, each containing nine fins. Within each quadrant, there is symmetry with respect to the diagonal, so that measurements made at the three fins which straddle the diagonal and at the three fins situated to either side of the diagonal yield all the needed information.

Array inlet and exit configurations

Attention is now turned to the modified array inlet and exit configurations that were investigated here. The original (unshrouded) inlet is that shown in Fig. 1. The square opening shown there has a side length $L = 7.684$ cm (3.025 in.). Of the two investigated shrouded inlets, the first was assigned a side length L_1 such that the opening area was one half that of the original opening area, that is, $L_1^2 = \frac{1}{2}L^2$ or $L_1 = 5.433$ cm (2.139 in.).

For certain of the array geometries, the use of the L_1 shroud led to the desired spatial uniformity of the per-fin mass transfer coefficient. However, in other cases, the actual shroud-related changes in the spatial distribution exceeded the intended changes. For those cases, a second shroud (the L_2 shroud) was employed whose opening area was intermediate to the openings of the original inlet and the L_1 shroud. The side length of the second shroud was $L_2 = 6.939$ cm (2.732 in.).

The geometrical relationships between the various shrouds can be seen in the lower part of Fig. 3. The figure shows the original square opening (side L) and the L_1 and L_2 openings. By making use of both the upper and lower parts of the figure, it can be seen that for all the three S/D values, the L_1 shroud blocks direct impingement of the incoming flow on the tips of the outermost fins of the array. On the other hand, the L_2 shroud provides full blockage of the outermost fins for the $S/D = 4.10$ array, but only partial blockage for the other S/D arrays.

The modified array exit configuration will now be considered. As shown in Fig. 2(c), the modification involved the use of a new baseplate which extended out beyond the original baseplate. The new baseplate was a square metal sheet whose side dimension L_3 was twice that of the side of the original baseplate, that is, $L_3 = 2L = 15.368$ cm (6.050 in.).

As seen in Fig. 2, the new baseplate rested on the original baseplate. It was drilled with 36 holes to accommodate the shanks of the fins. Baseplates were fabricated and used with the $S/D = 2$ and 4 fins. As will be documented shortly, the results of these experiments suggested that little useful information would be obtained were the $S/D = 1.5$ fins to be used with an extended baseplate and, accordingly, such experiments were not performed.

Experimental procedure

Each data run included a preparatory thermal equilibration period followed by the data run proper. During the equilibration period, air was passed through the array at the flow rate designated for the run, but the naphthalene-coated fin was shrouded by a Teflon cover to prevent sublimation. Once thermal equilibrium had been attained, the coated fin was removed from the array, weighed, returned to the array for a brief re-equilibration, and then uncovered to initiate the data run proper. At the end of the run, the coated fin was weighed again. After that, a mock data run was made to determine a correction ($\sim 2\%$) to account for possible extraneous mass losses during handling and during the re-equilibration period.

The insertion (extraction) of the coated fin into (from)

the array was accomplished with special gripping tools which enabled these operations to be performed in the presence of small interfin spacings (i.e. small S/D). However, even with these tools, the smallest feasible value of S/D was about 1.5.

The pressure drop through the array was measured in a set of data runs separate from the mass transfer runs. For these runs, the array was populated only by metallic fins.

DATA REDUCTION

The per-fin mass transfer coefficient K and its dimensionless counterpart, the Sherwood number Sh, were evaluated from the following equations of definition:

$$K = \dot{m}/(\rho_{nw} - \rho_{nb}), \quad Sh = KD/\mathscr{D}. \tag{2}$$

The quantity $\dot{m}$ is the rate of naphthalene mass transfer per unit surface area. It was found by dividing the measured change of mass of the coated fin by the surface area of the fin and the duration time of the run. The naphthalene vapor density at the fin surface ρ_{nw} was calculated from the Sogin vapor pressure equation in conjunction with the perfect gas law, while the vapor density ρ_{nb} in the bulk flow is zero in these experiments. To simplify the evaluation of the Sherwood number, the diffusion coefficient $\mathscr{D}$ was eliminated by introducing the Schmidt number $Sc = \nu/\mathscr{D}$ and noting that $Sc = 2.5$ for diffusion of naphthalene in air. This gives

$$Sh = 2.5KD/\nu. \tag{3}$$

The Reynolds number was defined so that for a given fin array, it would have a constant value at a fixed flow rate of air, regardless of the shrouding arrangement. Such a definition was motivated by the desire to compare the effect of shrouding on the Sherwood numbers for a given array, under the condition of constant airflow rate. In this regard, for each array, a reference velocity V was defined as

$$V = \dot{w}/\rho[L^2 - 36(\pi D^2/4)], \tag{4}$$

where $\dot{w}$ is the airflow rate through the array. The bracketed quantity appearing in equation (4) is the free-flow area encountered by the airstream as it enters the unshrouded array. This same reference velocity will be employed both in the absence and in the presence of a shroud. With V from equation (4), Re was defined as

$$Re = \rho VD/\mu. \tag{5}$$

To cast the array pressure drop Δp in dimensionless terms, the reference velocity of equation (4) is used to define a pressure loss coefficient K_p

$$K_p = \Delta p/\tfrac{1}{2}\rho V^2. \tag{6}$$

With this definition, changes in K_p due to shrouding for a given array and at fixed airflow rate are true reflections of changes in Δp.

SHERWOOD (NUSSELT) NUMBERS AND PRESSURE COEFFICIENTS

The per-fin Sherwood numbers for all the investigated fin arrays, inlet configurations, exit configurations, and Reynolds numbers will now be presented. In view of equation (1), these results can be readily transformed to Nusselt numbers for heat transfer to air. The results for the different inlets will be the first item of business, after which the effects of the exit modification will be explored. This will be followed by a tabulation of the array pressure drop coefficient.

Sh results for the various inlets

In Figs. 4–9, the per-fin Sherwood number is plotted as a function of the Reynolds number for a specific array

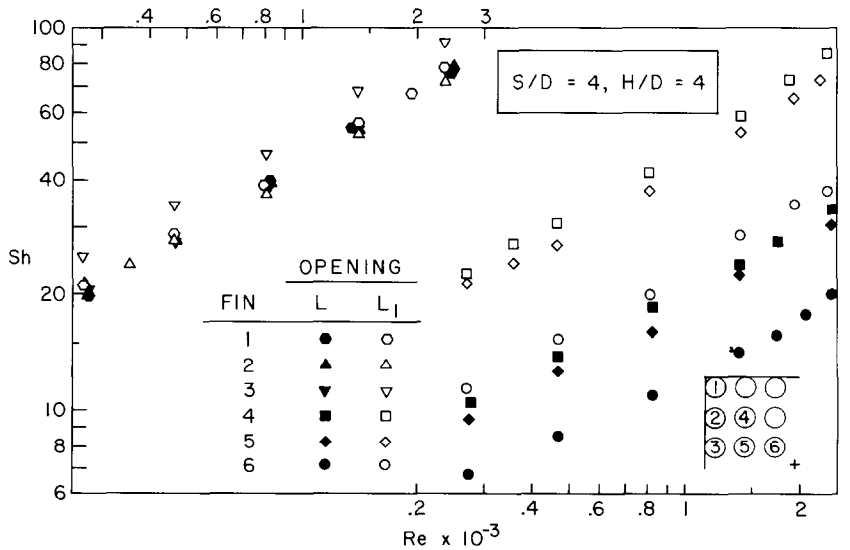

FIG. 4. Per-fin Sherwood number results for various inlet configurations, $S/D = 4$, $H/D = 4$.

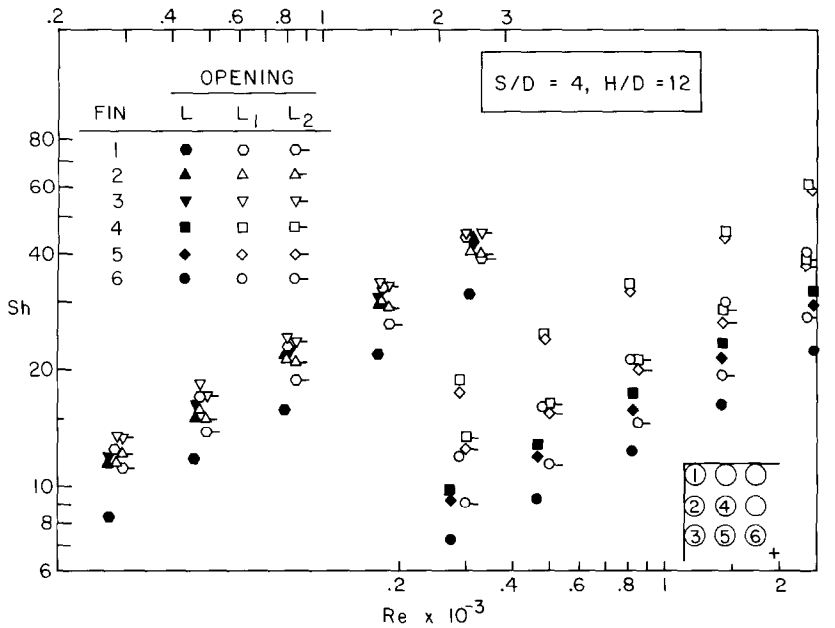

FIG. 5. Per-fin Sherwood number results for various inlet configurations, $S/D = 4$, $H/D = 12$.

configuration characterized by given values of S/D and H/D. Among these, Figs. 4 and 5 are for the thinnest fins ($S/D = 4$), Figs. 6 and 7 are for the intermediate thickness fins ($S/D = 2$), and Figs. 8 and 9 are for the thickest fins ($S/D = 1.5$). For each pair of figures, the first is for the shorter fins $H/D = 4$ and the second is for the longer fins $H/D = 12$.

Each figure conveys a substantial amount of information, and it is appropriate first to explain the format of the figure before going on to the technical content. The first point to be made is that a knowledge of the Sherwood numbers at six fin locations is sufficient to establish the Sherwood number results at all 36 fins in the array. In this regard, note has already been taken of the quadrant symmetry of the array (Fig. 1). A quadrant of the array is shown in the lower right-hand corner in each of Figs. 4–9. Within each quadrant, there is symmetry with respect to the diagonal, so that the three fins to one side of the diagonal are mirror images of the three fins to the other side. Thus, measurement of the transfer characteristics along the diagonal and to either side of the diagonal specifies the transfer characteristics of all nine fins in the quadrant and, by quadrant symmetry, of all 36 fins in the array.

The aforementioned quadrant diagrams in each figure indicate the numbering system for the six fundamental fin positions. Throughout the discussion of the results, fins 1–3 will be referred to as the edge-adjacent or exterior fins, while fins 4–6 will be called the interior fins.

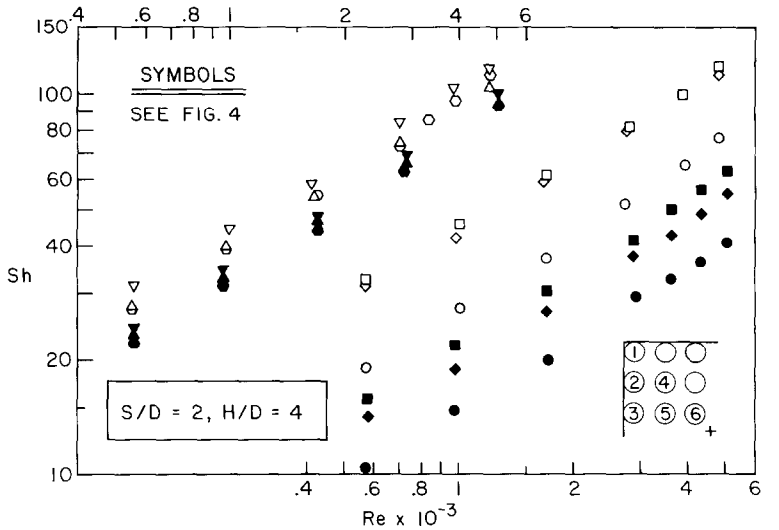

FIG. 6. Per-fin Sherwood number results for various inlet configurations, $S/D = 2$, $H/D = 4$.

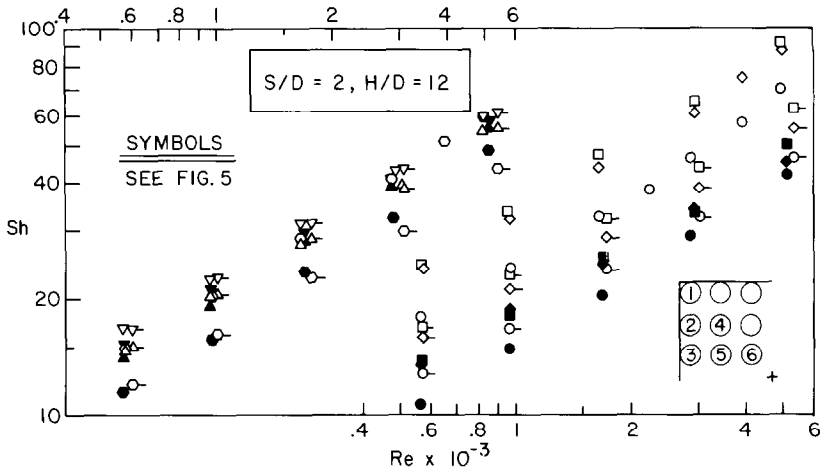

FIG. 7. Per-fin Sherwood number results for various inlet configurations, $S/D = 2$, $H/D = 12$.

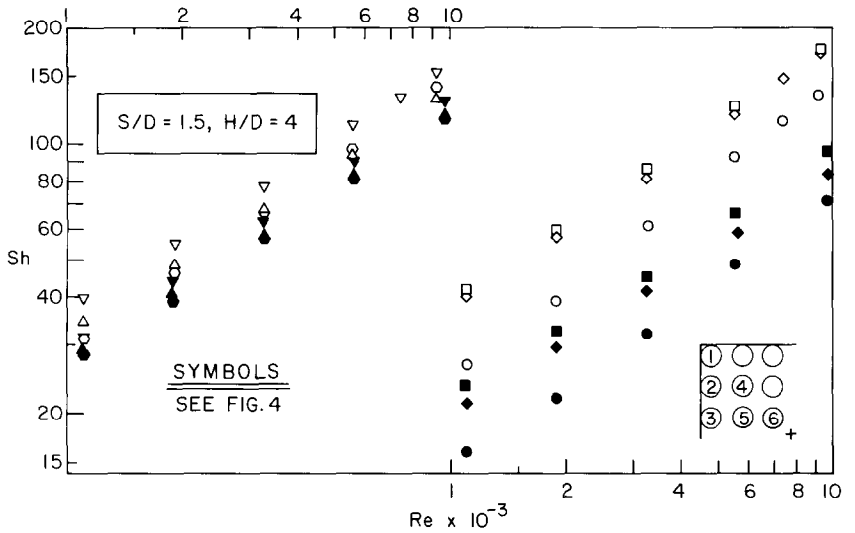

FIG. 8. Per-fin Sherwood number results for various inlet configurations, $S/D = 1.5$, $H/D = 4$.

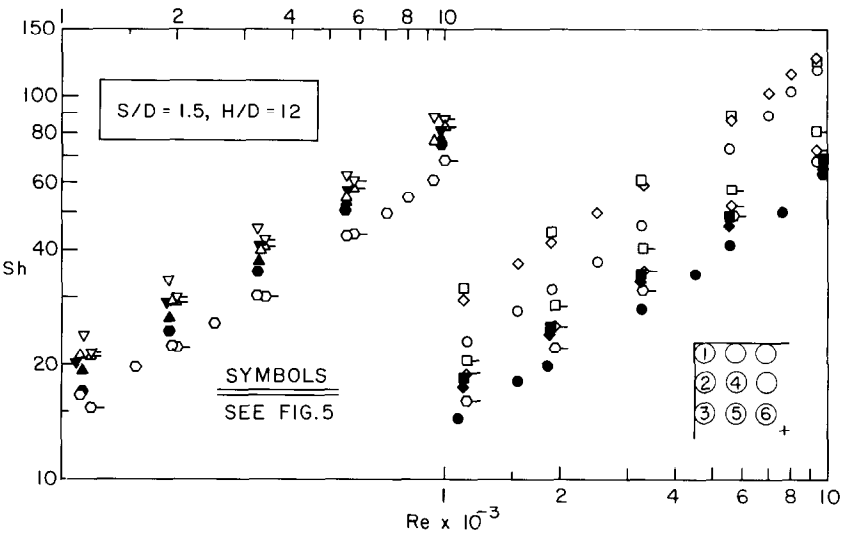

FIG. 9. Per-fin Sherwood number results for various inlet configurations, $S/D = 1.5$, $H/D = 12$.

The Sherwood number results for the edge-adjacent fins are plotted in the left-hand portion of each figure, while the results for the interior fins are plotted in the right-hand portion. The reason for separating the results in this way is to avoid congestion and also to make easier the identification of the different responses of the edge-adjacent fins and the interior fins to shrouding. The data for the edge-adjacent fins are referred to the Reynolds number scale that runs along the abscissa on the upper left of each figure; the Reynolds number scale for the interior fins runs along the abscissa on the lower right. All fins are referred to the same ordinate scale for the Sherwood number. The matching up of the edge-adjacent and interior fin data for the same Reynolds number is easily accomplished by counting data clusters, starting from the left and working toward the right along the upper and lower abscissa scales.

In each figure, data are presented for the various inlet configurations as indicated in the legend. The unshrouded inlet is designated as the L inlet opening, while the two shrouded inlets are identified as the L_1 and L_2 openings (these openings are displayed in the lower part of Fig. 3). Note that for a given array, a given Reynolds number corresponds to the same airflow rate for both the unshrouded and shrouded arrays.

Attention will first be turned to the results for the unshrouded arrays (black symbols) since they serve as baseline information against which the results for the shrouded arrays will be compared. Aside from the data for the $S/D = 1.5$ arrays, the Sherwood number results for the other unshrouded arrays were presented in ref. [1] and are discussed there in detail. Therefore, only the major trends need be identified here. In general, the Sherwood numbers at the exterior fins exceed those at the interior fins [except, in certain instances, for relatively low values at the corner fin (fin 1)]. At a given interfin spacing S/D, the interior/exterior differences are accentuated for shorter fins, as also occurs for larger S/D for a given fin height H/D.

Among the interior fins, the Sherwood number at the most-centered fin (fin 6) is lowest, while that at fin 4 is generally highest although it does not differ much from the Sherwood number at fin 5. For the exterior fins, the Sherwood numbers at fins 2 and 3 are almost always in close accord. The corner fin 1 behaves rather inconsistently in that its Sherwood number is equal to those at fins 2 and 3 for some arrays but is lower for other arrays.

The higher transfer coefficients at the exterior fins can be attributed to the fact that those fins are washed by the full airflow rate while the interior fins are washed by only part of the airflow. To obtain more uniform coefficients, it appears appropriate to redirect the airflow so that more of it washes over the interior fins, and this can be accomplished by shrouding. With a shroud in place, the exterior fins will continue to be washed by the full flow, albeit with a different pattern. Thus, it can be expected that shrouding will more greatly affect the coefficients at interior fins than at the exterior fins.

With this as background, the results for the L_1 shroud [the more covering of the two shrouds (see Fig. 3)] will now be considered. These results are represented by the open data symbols in Figs. 4–9. From the figures, it is seen that at a fixed Reynolds number (fixed airflow rate), the presence of the shroud brings about a significant increase in the Sherwood numbers at the interior fins. The increase, in the range of a factor of two, is relatively uniform at the three interior fin locations 4–6.

At the exterior fins, there is an overall tendency toward higher coefficients in the presence of the L_1 shroud, but the effect is smaller and less regular than at the interior fins. Generally, the with-shroud coefficients do not deviate by more than 25% from the no-shroud values.

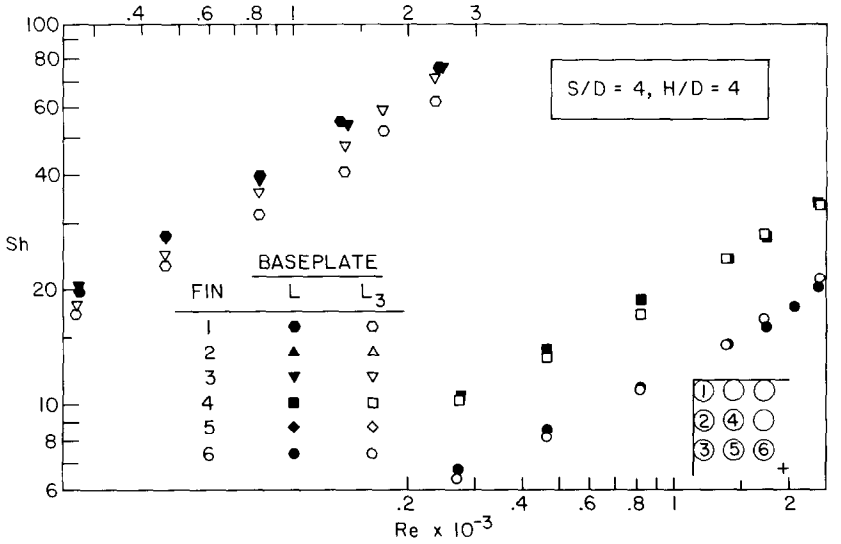

FIG. 10. Effect of extended baseplate on the per-fin Sherwood number, $S/D = 4$, $H/D = 4$.

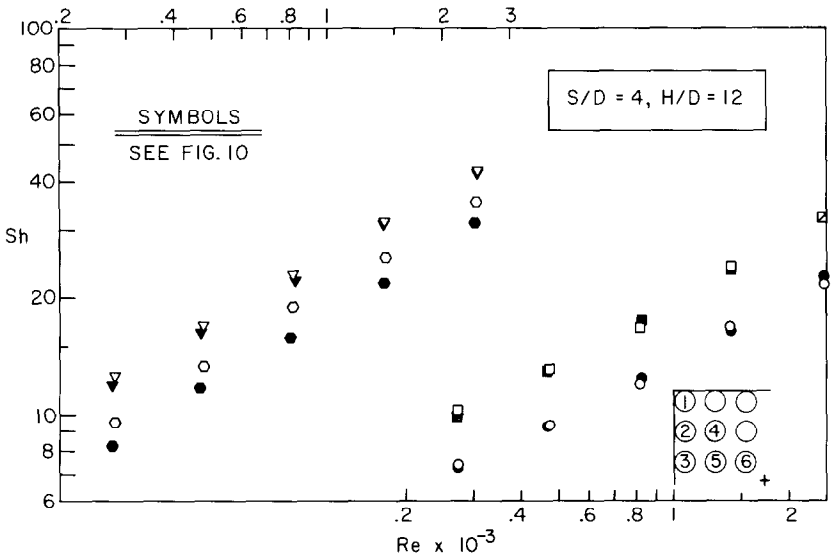

FIG. 11. Effect of extended baseplate on the per-fin Sherwood number, $S/D = 4$, $H/D = 12$.

For those arrays where there were large interior/exterior Sherwood number variations for the unshrouded case, the presence of the L_1 shroud brings about near spatial uniformity of the transfer coefficients (aside from the individualistic behavior of fin 6). This outcome can be seen in Figs. 4, 6, and 8. On the other hand, for those arrays with more moderate interior/exterior variations for the unshrouded case, the L_1 shroud brings about a reverse imbalance of the coefficients, that is, the coefficients at the interior fins exceed those at the exterior fins. The reversal can be observed in Figs. 5, 7, and 9. Thus, for those cases, the blockage provided by the L_1 shroud is greater than what is needed to attain spatial uniformity.

Experiments were performed for those cases using the less-covering L_2 shroud (Fig. 3). As expected and documented in Figs. 5, 7, and 9, the Sherwood numbers are less affected by the L_2 shroud than by the L_1 shroud, especially at the interior fins. In general, the use of the L_2 shroud provided satisfactory spatial uniformity for those cases for which it was employed.

The results of Figs. 4–9 indicate that shrouding of the array inlet can promote spatial uniformity while generally increasing the level of the Sherwood numbers for the array as a whole. As will be documented later, these gains are purchased at the expense of a pressure drop increase, so that a performance analysis is needed to assess the practical utility of inlet shrouding.

Sh results for the extended baseplate

The array exit modification utilizing an extended baseplate is shown schematically in Fig. 2(c). It is expected that for arrays where there is strong channeling of the flow in the array brought about by tall and/or closely spaced fins, the baseplate extension should have a smaller effect than for more open arrays. Also, the exterior fins should be more affected than the interior fins.

The presentation will begin with the array for which the least channeling is expected, namely, $S/D = 4$ and $H/D = 4$, and Fig. 10 has been prepared for this purpose. The format of Fig. 10 is similar to that of Figs. 4–9. Open data symbols have been used to distinguish the results for the extended baseplate (i.e. L_3 baseplate) from the results for the standard baseplate (i.e. L baseplate) represented by black data symbols. Note that data are presented at only four fin locations rather than the usual six. This is because the close pairing of the results for fins 4 and 5 and for fins 2 and 3 obviates the need to show the data for all locations and, specifically, extended-baseplate data were not collected for fins 2 and 5.

Inspection of Fig. 10 indicates that the interior-fin Sherwood numbers are virtually unaffected by the extended baseplate. On the other hand, there are readily detectable effects at the exterior fins. Not unexpectedly, the corner fin 1 is most affected, and 20–30% changes in the Sherwood number occur at that location. At fin 3, the baseplate-related change in the Sherwood number is about 10%.

Figure 11 shows results for the same S/D as in Fig. 10 but for taller fins (i.e. for $H/D = 12$). Here, more channeling is expected than in the previous case. The interior fins continue to be insensitive to the extended baseplate, and this insensitivity now also prevails at the exterior fin location 3. Only the corner fin 1 responds to the baseplate but to a lesser extent (15–20%) than for the lower fins. In testimony to the maverick nature of the corner fin, Fig. 11 shows a baseplate-related increase while Fig. 10 shows a decrease.

Consideration is next given to a more tightly spaced array (i.e. $S/D = 2$), and results for the low-fin version of this array are presented in Fig. 12. The tighter spacing should result in greater channeling. In this regard, it is relevant to compare Figs. 10 and 12, which have the same H/D but which differ in the tightness of the fin

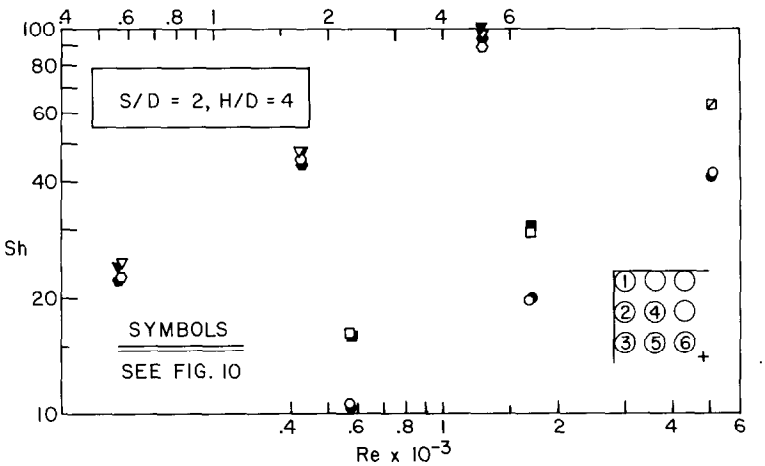

FIG. 12. Effect of extended baseplate on the per-fin Sherwood number, $S/D = 2$, $H/D = 4$.

spacing. Clearly, the more tightly spaced array (Fig. 12) is less sensitive to the extended baseplate.

Experiments performed for the tall-fin counterpart of Fig. 12 displayed results that were altogether unaffected by the extended baseplate. Since the baseplate effects for the $S/D = 1.5$ case should be even smaller than those for the $S/D = 2$ case, it was not deemed necessary to carry out experiments for the former.

In summary, it appears that the fin transfer coefficients are affected by the array exit configuration only for open arrays, and then only at the exterior fins.

Pressure loss coefficients

Array pressure drops, expressed in terms of the pressure loss coefficient K_p of equation (6), are presented in Table 1. For any given array geometry, K_p was found to be nearly independent of the Reynolds number. The slight Reynolds-number-related variations were averaged out, and it is the average values which are listed in the table.

Upon reviewing the definition of the velocity V [i.e. equation (4)] that appears in the denominator of K_p, it is clear that all arrays characterized by a common value of S/D will have the same value of V at a given rate of airflow. Thus, variations among the K_p values for the various arrays which have a common value of S/D are true reflections of the variations of Δp at a given airflow rate. However, comparisons between K_p values for arrays with different values of S/D are not truly indicative of differences in Δp, since the velocities are different.

Inspection of the table shows that, as expected, shrouding of the inlet leads to an increase in the array pressure drop, with the increase being greater as the open area decreases. Perhaps less expected is the fact that for a given S/D and given inlet and exit configurations, the pressure drop decreases as the fin height H increases. The decrease in the pressure drop is due to the lowering of the velocity within the array and at the exit plane (the array exit area is proportional to the fin height H).

The effect of the extended baseplate (i.e. the L_3 base) on the pressure drop is small. For three of the four cases listed in the table, the pressure drop is increased by the presence of the extended baseplate, while in the fourth case it is decreased. In this regard, it may be observed that the separation distance between the array inlet and the baseplate (i.e. the height H) is larger for the latter case than for the other three. In supplementary experiments involving the two baseplates without fins, it was found that the pressure drop for the extended baseplate exceeded that for the standard baseplate at small and intermediate separation distances, but that there was a reversal at larger separations. This finding reinforces the pressure drop results obtained for the fin arrays.

ANALYTICAL MODEL FOR HEAT TRANSFER

A model will now be formulated which will facilitate the application of the measured per-fin Sherwood numbers to the calculation of the overall rate of heat

Table 1. Pressure loss coefficient K_p

S/D	H/D	Unmodified	L_1 inlet	L_2 inlet	L_3 base
1.5	4	3.87	10.3		
	12	2.34	8.58	2.91	
2	4	4.73	13.9		5.09
	12	2.46	9.99	3.53	2.40
4	4	8.81	24.5		9.26
	12	2.99	11.5	4.51	3.10

transfer from the array to an airstream passing through the array. The development will be couched in heat transfer terms and, in this regard, the per-fin Sherwood numbers will be regarded as being transformed to per-fin Nusselt numbers by means of equation (1).

The overall rate of heat transfer is obtained by summing the rates of heat transfer at the individual pin fins. In calculating the latter, the bulk temperature of the air adjacent to each fin is needed. As noted in the Introduction, the determination of the distribution of the bulk temperature throughout the array is a major point of difficulty. The difficulty stems from the fact that the same rate of airflow does not wash over each fin, so that the first law of thermodynamics cannot be applied in a straightforward manner to obtain the bulk temperature distribution.

As a first approximation, the bulk temperature may be regarded as being uniform throughout the array, equal either to the inlet value T_{bi}, or to the exit value T_{be}, or to the inlet-exit average $T_{ba} = \frac{1}{2}(T_{bi} + T_{be})$. If all the fins are assumed to be at the same uniform temperature T_w, then, at any fin j, the rate of heat transfer Q_j is given by

$$Q_j = h_j A(T_w - T_{bi}), \quad Q_j = h_j A(T_w - T_{be}), \quad Q_j = h_j A(T_w - T_{ba}), \tag{7}$$

respectively for each of the assumed constant values of T_b. In equation (7), h_j is the local, per-fin heat transfer coefficient, and A is the fin surface area which is common to all fins.

The overall rate of heat transfer Q from the entire array then follows as

$$Q = \sum_{j=1}^{36} Q_j. \tag{8}$$

For the $T_b = T_{bi}$ assumption, equation (8) and the first of equations (7) yield the value of Q. However, for the $T_b = T_{be}$ assumption, the first law of thermodynamics has to be used to determine T_{be}, that is

$$Q = \dot{w} c_p (T_{be} - T_{bi}). \tag{9}$$

Simultaneous solution of equations (9) and (8), with q_j from the second of equation (7), yields T_{be} and, thereafter, Q. A similar approach is used for the $T_b = T_{ba}$ assumption.

A better representation of the bulk temperature distribution can be achieved with a zonal model, whereby the array is subdivided into zones within which the bulk temperature is a constant. A three-zone model will be employed here, and the zonal layout for the case of the unshrouded inlet is shown in Fig. 13. As seen there, the zone boundaries are positioned midway between the tiers of fins. The inner, middle, and outer zones are designated as I, II, and III, respectively.

In addition to incorporating a zone-to-zone variation of the bulk temperature, the computational model will also take account of temperature variations along the height of the fins. This is accomplished via the

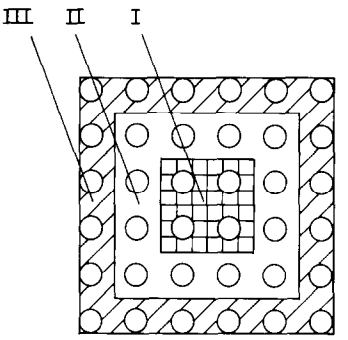

FIG. 13. Zonal layout for the case of the unshrouded inlet.

fin efficiency η. For fin j, the expression used for the efficiency (found in standard textbooks) is

$$\eta_j = \frac{1 + (m_j k_f / h_j) \tanh (m_j H)}{(1 + 4H/D)[1 + (h_j / m_j k_f) \tanh (m_j H)]}, \tag{10}$$

where

$$m_j = (4h_j / k_f D)^{1/2}, \tag{11}$$

and k_f denotes the thermal conductivity of the fins. It will be assumed that the fin base temperature is identical for all fins and is equal to T_w.

In the analysis, it will be convenient to use the abbreviations

$$h_I = \sum_I \eta_j h_j, \quad h_{II} = \sum_{II} \eta_j h_j, \quad h_{III} = \sum_{III} \eta_j h_j. \tag{12a}$$

Note that in terms of the notation of Figs. 4–9

$$h_I = 4\eta_6 h_6, \quad h_{II} = 4(\eta_4 h_4 + 2\eta_5 h_5), \quad h_{III} = 4[\eta_1 h_1 + 2(\eta_2 h_2 + \eta_3 h_3)]. \tag{12b}$$

A key feature of the model is the rate at which airflow enters each zone at the array inlet. In this regard, let $\hat{A}_I$, $\hat{A}_{II}$, and $\hat{A}_{III}$ denote the inlet free-flow areas for zones I, II, and III, respectively, and let $\hat{A}$ denote their sum. Then, the respective entering flows are calculated from

$$\dot{w}_I = (\hat{A}_I / \hat{A})\dot{w}, \quad \dot{w}_{II} = (\hat{A}_{II} / \hat{A})\dot{w}, \quad \dot{w}_{III} = (\hat{A}_{III} / \hat{A})\dot{w}. \tag{13}$$

Energy balances are then made for each zone. For zone I

$$Q_I = h_I A(T_w - T_{bI}) = \dot{w}_I c_p (T_{bI,e} - T_{bi}). \tag{14}$$

In the energy balance for zone II, cognizance has to be taken of two inflows, one from the array opening and the other from zone I. Therefore

$$Q_{II} = h_{II} A(T_w - T_{bII}) = \dot{w}_{II} c_p (T_{bII,e} - T_{bi}) + \dot{w}_I c_p (T_{bII,e} - T_{bI,e}). \tag{15}$$

Similarly, for zone III

$$Q_{III} = h_{III} A(T_w - T_{bIII}) = \dot{w}_{III} c_p (T_{bIII,e} - T_{bi}) + (\dot{w}_I + \dot{w}_{II}) c_p (T_{bIII,e} - T_{bII,e}). \tag{16}$$

The terms appearing in these equations are generally familiar, except perhaps for $T_{bI,e}$, $T_{bII,e}$, and $T_{bIII,e}$. These terms denote the bulk temperatures of the air leaving zones I, II, and III, respectively.

As written, equations (14)–(16) contain six unknowns: T_{bI}, T_{bII}, T_{bIII}, $T_{bI,e}$, $T_{bII,e}$, and $T_{bIII,e}$. It is, therefore, necessary to specify three relationships between them. Perhaps the simplest set is

$$T_{bI} = T_{bI,e}, \quad T_{bII} = T_{bII,e}, \quad T_{bIII} = T_{bIII,e}, \tag{17}$$

and these were employed here.

With equation (17), the solution of equations (14)–(16) is straightforward. Equation (14) is solved for $T_{bI,e}$, which is introduced into equation (15). That equation is, in turn, solved for $T_{bII,e}$. Then, $T_{bII,e}$ is substituted into equation (16), which yields $T_{bIII,e}$. These operations can be performed algebraically to give fairly compact expresssions for the temperatures. Once these temperatures have been found, Q_I, Q_{II}, and Q_{III} follow from equations (14)–(16), again in algebraic form, if desired. The array heat transfer rate is then obtained by summing

$$Q = Q_I + Q_{II} + Q_{III}. \tag{18}$$

The only aspect of the foregoing computational model which has to be tuned in the presence of the inlet shrouds is the determination of the mass flows $\dot{w}_I$, $\dot{w}_{II}$, and $\dot{w}_{III}$. For the L_1 shroud (lower part of Fig. 3), the boundary between regions II and III was chosen to coincide with the edge of the shroud, so that $\hat{A}_{III} = 0$ and $\hat{A} = \hat{A}_I + \hat{A}_{II}$. In the case of the L_2 shroud (the narrower shroud), the boundaries between the zones were positioned as in the no-shroud case, with proper account being taken of the differences in the $\hat{A}_3$ values for the two cases. No modifications need be made for the case of the extended baseplate.

The foregoing computational model is believed to be an effective tool for employing the measured per-fin Sherwood numbers for the determination of the overall rate of heat transfer from the array. It will be used in the performance evaluations to be presented shortly.

PERFORMANCE EVALUATIONS

It remains to compare the heat transfer performance of the various arrays for which data have been collected. The performance comparison depends on the conditions under which the arrays are being compared. A commonly used condition of comparison is that the pumping power P be equal for the various arrays. If $\dot{V}$ denotes the volume flow rate of the air passing through the array, then the pumping power is given by

$$P = \dot{V}\Delta p, \tag{19}$$

where Δp is the array pressure drop.

For a specified value of P, equation (19) constitutes a relation between $\dot{V}$ and Δp which, when matched with the K_p value of a given array (Table 1), yields the airflow rate for the array and the corresponding Reynolds number. In general, for a fixed value of the pumping power, the Reynolds numbers for the various arrays will be different, and the Sherwood (Nusselt) numbers used in the heat transfer calculations have to be taken at the appropriate Reynolds numbers.

At each of several fixed values of the pumping power, comparisons will be made of the overall rate of heat transfer from various arrays. The compared heat transfer rates correspond to a common value of $(T_w - T_{bi})$ for all arrays.

Before proceeding with the details of the performance evaluation, it should be noted that many other constraints can be employed instead of equal pumping power. For example, in industrial practice, it may be that a given blower has been selected, and it is desired to choose a heat exchanger configuration which gives the best performance when mated with the blower. In that case, the blower performance curve

$$\dot{V} = f(\Delta p), \tag{20}$$

would serve as the constraint, replacing equation (19). Indeed, equation (19) is a special case of equation (20), with $f(\Delta p) = \text{const.}/\Delta p$. Because of this, the methodology used for employing equation (19), to be described shortly, will also serve for equation (20).

In the presentation which follows, the array-to-array Reynolds number differences corresponding to the equal pumping power constraint will be determined first, after which the heat transfer from the arrays will be computed and compared.

Reynolds number comparisons

If it is noted that $\dot{V} = \dot{w}/\rho$, then the pumping power P of equation (19) can be rephrased using equations (4)–(6), with the result

$$P/(\tfrac{1}{2}\mu^3/\rho) = K_p Re^3[L^2 - 36(\pi D^2/4)]/D^3. \tag{21}$$

Equation (21) may be used to implement the equal pumping power condition for two arrays A and B. If the two arrays have the same value of S/D, then

$$Re_A = Re_B(K_{pB}/K_{pA})^{1/3}, \tag{22}$$

whereas for arrays with different S/D

$$Re_A = Re_B(K_{pB}/K_{pA})^{1/3}(D_A/D_B)[L^2 - 9\pi D_B^2]^{1/3}/[L^2 - 9\pi D_A^2]^{1/3}, \tag{23}$$

where it has been assumed that the properties μ and ρ are the same for the two arrays. Thus, if Re_B is specified, then Re_A can be determined from equation (22) or equation (23).

Table 2 has been prepared to illustrate the Reynolds numbers obtained from the equal pumping power condition. The table is subdivided into three parts, respectively for fixed values of $S/D = 1.5$, 2, and 4. For each S/D, three representative values of the Reynolds number have been assigned for the unshrouded array with $H/D = 12$. These Reynolds numbers are listed in the left-hand column of the table. For the various other arrays designated in the successive column headings,

Table 2. Equal pumping power Reynolds numbers*

$Re(12)$	$Re(12, L_1)$	$Re(12, L_2)$	$Re(4)$	$Re(4, L_1)$
		(a) $S/D = 1.5$		
3000	1945	2790	2537	1830
5000	3240	4650	4230	3050
9000	5832	8369	7614	5490
		(b) $S/D = 2$		
1800	1128	1596	1448	1010
3000	1881	2660	2412	1683
5000	3135	4433	4020	2805
		(c) $S/D = 4$		
800	510	698	558	397
1500	956	1308	1046	744
2500	1595	2180	1745	1240

* The parentheses adjacent to Re designate the H/D and the shroud.

there are listed the constant pumping power Reynolds numbers which correspond to the aforementioned Reynolds number values for the $H/D = 12$ unshrouded array. All the arrays considered in Table 2 have the standard (i.e. unmodified) baseplate.

The second and third columns of Table 2, in common with the first column, pertain to $H/D = 12$, and the entries in these columns reflect the effect of shrouding. Successively, these columns correspond to the unshrouded array, the L_1 shroud opening, and the L_2 shroud opening. As expected, for a fixed pumping power, arrays with shrouded inlets operate at lower Reynolds numbers than the unshrouded case. The Reynolds numbers for the L_1 shrouded arrays are 62–65% of those for the unshrouded arrays, while those for the L_2 shrouded arrays are about 90% of the unshrouded values.

The fourth and fifth columns of the table respectively pertain to the unshrouded and the L_1 shrouded arrays with $H/D = 4$. A comparison of the Reynolds numbers in these columns with those in the first and second columns shows the effect of fin height. The observed lower Reynolds numbers for $H/D = 4$ relative to those for $H/D = 12$ are consistent with the higher K_p values for the former (Table 1).

Heat transfer comparisons

The rates at which heat is transferred from various arrays operated at the same pumping power and at the same value of $(T_w - T_{bi})$ will now be compared. The heat transfer rates were computed using the methodology developed earlier in the paper, and Tables 3 and 4 have been prepared to convey this information. The results in Table 3 are for fins with an efficiency $\eta = 1$, while those of Table 4 are for aluminum fins ($k_f = 228$ W m^{-1} °C^{-1}) whose efficiency is calculated from equation (10). The thermal conductivity of air used in computation of Q was 0.0258 W m^{-1} °C^{-1}. All of the arrays dealt with in Tables 3 and 4 have the standard (i.e. unmodified) baseplate.

Each of the tables is subdivided into three parts, respectively for fixed values of $S/D = 1.5$, 2, and 4. The Reynolds number entries on the LHS of each table are the very same as appear in the left-hand column of Table 2. Those Reynolds numbers yielded equal pumping power Reynolds numbers for various arrays (see Table 2), and these Reynolds numbers were used as input information to compute the heat transfer rate for the respective arrays. Thus, the specified first-column Reynolds number serves, in effect, to fix the level of the pumping power for all the entries in the line of the table in which it is situated.

The heat transfer results presented in Tables 3 and 4 are in ratio form, with the numerator and denominator corresponding to different arrays whose H/D and shrouding condition are indicated in parentheses (the no-shroud condition is undesignated). The deviation of the ratio from unity is a measure of the relative heat transfer performance of the arrays being compared.

The second column of the table compares the $H/D = 12$ array having an L_1 inlet shroud to the $H/D = 12$ array without an inlet shroud. The resulting Q ratios do not differ very much from one (maximum deviations ~6–7%), but there is a trend with S/D whereby the presence of the L_1 shroud reduces the heat transfer at the smallest S/D and increases the heat transfer at the largest S/D. In the next column of the table, a comparison is made between the $H/D = 12$ array having an L_2 inlet shroud and the $H/D = 12$ array without a shroud. For all the S/D investigated, the Q ratio is nearly equal to one. Thus, it appears that for the tallest fins ($H/D = 12$), from the standpoint of the array heat transfer rate, there is no clear advantage in shrouding the inlet.

Attention is next turned to the last column of Tables 3 and 4, where another shroud/no-shroud comparison is made. In this case, the comparison is between the $H/D = 4$ array having an L_1 inlet shroud and the $H/D = 4$ array without a shroud. The Q ratios fall in the range 1.1–1.15, indicating enhancement for the span of S/D

Table 3. Equal pumping power heat transfer rates. Fin efficiency $\eta = 1$*

$R(12)$	$\frac{Q(12, L_1)}{Q(12)}$	$\frac{Q(12, L_2)}{Q(12)}$	$\frac{Q(4)}{Q(12)}$	$\frac{Q(4, L_1)}{Q(4)}$
		(a) $S/D = 1.5$		
3000	0.938	1.009	0.499	1.112
5000	0.953	1.014	0.496	1.137
9000	0.972	1.028	0.490	1.145
		(b) $S/D = 2$		
1800	0.982	1.004	0.465	1.153
3000	0.987	0.994	0.472	1.138
5000	0.991	0.993	0.471	1.142
		(c) $S/D = 4$		
800	1.056	0.991	0.443	1.106
1500	1.065	0.997	0.449	1.094
2500	1.072	1.017	0.454	1.104

* The parentheses adjacent to Q designate H/D and the shroud.

investigated. Thus, for shorter fins, shrouding appears advantageous.

A comparison between the rates of heat transfer from tall and short fins is made in the fourth column of the table. The comparison corresponds to unshrouded arrays. The taller fins are clearly advantageous, but to a lesser extent for the aluminum fins ($\eta \neq 1$) than for the ideal fins ($\eta = 1$). Another comparison (not shown in the tables) indicates that for a fixed H/D, higher heat transfer rates occur for smaller S/D, with the largest values corresponding to $S/D = 1.5$. When the arrays being compared had the same H/D, the computed Q ratios were insensitive to the fin efficiency.

CONCLUDING REMARKS

This paper has conveyed experimental per-fin heat transfer coefficients and overall pressure drop results for a novel pin-fin arrangement and has set forth a computational method for determining the heat transfer rate for the array as a whole. The method, which utilizes the measured heat transfer and pressure drop information, was employed to facilitate a comparison of the performance of the various investigated arrays. The novelty of the arrangement stems from the fact that fluid enters the array at the plane of the fin tips. The fluid at first penetrates the array as a longitudinal flow, but it is forced to turn because of the blocking action of the array baseplate and exits the array in crossflow relative to the fins at the outer edges of the baseplate.

The experimental work had three foci. The first was to determine heat transfer and pressure drop results for arrays with more closely spaced fins than had been investigated in the past. Interest in closely spaced fins was motivated by performance comparisons which indicated that arrays with more closely spaced, larger diameter fins yielded higher rates of heat transfer at fixed pumping power than did more open arrays.

Table 4. Equal pumping power heat transfer rates. Fin efficiency from equation (10)*

$R(12)$	$\frac{Q(12, L_1)}{Q(12)}$	$\frac{Q(12, L_2)}{Q(12)}$	$\frac{Q(4)}{Q(12)}$	$\frac{Q(4, L_1)}{Q(4)}$
		(a) $S/D = 1.5$		
3000	0.952	1.007	0.630	1.106
5000	0.965	1.010	0.671	1.130
9000	0.980	1.019	0.729	1.130
		(b) $S/D = 2$		
1800	0.983	1.003	0.579	1.148
3000	0.987	0.996	0.625	1.133
5000	0.992	0.995	0.669	1.134
		(c) $S/D = 4$		
800	1.046	0.996	0.528	1.106
1500	1.051	1.002	0.568	1.095
2500	1.054	1.018	0.607	1.107

* The parentheses adjacent to Q designate H/D and the shroud.

In the second phase of the experiments, the inlet cross section of the array was partially shrouded in order to tailor the pattern of fluid flow. Two shrouds with different opening areas were employed. With the use of one or the other of these shrouds, it was possible to obtain nearly uniform per-fin heat transfer coefficients throughout the array.

The final set of experiments dealt with the possible effects of modifications in the exit geometry of the array. The specific modification that was investigated was an extension of the baseplate well beyond the outermost row of fins. It was found that the fin heat transfer coefficients were affected by the extended baseplate only for open arrays and then only at the outermost row of fins.

The key issue in formulating a computational model for the array heat transfer is the fact that the same rate of airflow does not wash over all of the fins, which makes it difficult to determine the bulk temperature distribution throughout the array. The model employed here subdivides the array into discrete zones within which the bulk temperature is a constant. In addition to the zonal distribution of the bulk temperature, the model also takes account of temperature variations along the fins.

Comparisons were made of heat transfer rates for various arrays operating at equal pumping power and equal baseplate to inlet-air temperature differences. At a given interfin spacing and fin diameter, taller fins yielded higher rates of heat transfer. The rate of heat transfer also increased with decreasing S/D at fixed H/D. Inlet shrouding proved to be advantageous for shorter fins.

REFERENCES

1. E. M. Sparrow and E. D. Larson, Heat transfer from pin fins situated in an oncoming longitudinal flow which turns to crossflow, *Int. J. Heat Mass Transfer* **25**, 603–614 (1982).
2. E. D. Larson and E. M. Sparrow, Performance comparisons among geometrically different pin-fin arrays situated in an oncoming longitudinal flow, *Int. J. Heat Mass Transfer* **25**, 723–725 (1982).

EFFET D'ENTREE, DE SORTIE ET DE GEOMETRIE D'AILETTE SUR DES AILETTES A PICOTS SITUEES DANS UN ECOULEMENT TOURNANT

Résumé—On considère des arrangements de picots cylindriques avec de l'air entrant dans l'arrangement par le plan des sommets des ailettes, tournant comme il traverse l'arrangement et sortant en écoulement croisé. Le coefficient de transfert thermique par ailette et les pertes de charge globales sont déterminés expérimentalement. Un modèle numérique est formulé pour déterminer les flux thermiques en tenant compte du fait que le même débit d'air ne lave pas toutes les ailettes dans le réseau. Le modèle est employé pour comparer les flux de chaleurs transférés pour différents arrangements avec des puissances égales de pompage. Les points particuliers du travail concernent l'étude des effects des géométries différentes d'entrée et de sortie du fluide et aussi l'utilisation d'un espacement de picots plus serré que dans le passé. On montre que le capotage partiel de l'entrée peut augmenter de façon presque uniforme les coefficients de transfert thermique par ailette à travers l'arrangement. Des modifications de la géométrie de sortie affecte seulement les arrangements les moins serrés et seulement à la rangée extrême d'ailettes.

EINFLUSS DER EINTRITTS-, AUSTRITTS- UND RIPPENGEOMETRIE AUF STIFTRIPPEN IN EINER UMGELENKTEN STRÖMUNG

Zusammenfassung—Es werden Anordnungen zylindrischer Stiftrippen betrachtet. Dabei tritt Luft in der Ebene der Rippenspitzen in die Anordnung ein. Der Luftstrom wird beim Durchströmen der Anordnung umgelenkt und verläßt diese im Querstrom. Der mittlere Wärmeübergangskoeffizient an den Rippen und der Druckabfall wurden experimentell bestimmt. Ein Rechenmodell zur Ermittlung des Wärmeübergangs in der Anordnung wurde formuliert, das die Tatsache berücksichtigt, daß nicht sämtliche Rippen der Anordnung von derselben Luftmenge umströmt werden. Das Modell wurde dazu verwendet, den Wärmeübergang in unterschiedlichen Anordnungen zu vergleichen, die bei derselben Gebläseleistung und bei derselben Temperaturdifferenz zwischen Grundplatte und Lufteintritt betrieben werden. Besondere Schwerpunkte der Arbeit waren, den Einfluß unterschiedlicher Eintritts- und Austritts-Geometrien der Strömung zu untersuchen und kleinere Rippenteilungen zu verwenden als bisher üblich. Es wird gezeigt, daß ein partielles Abdecken des Eintritts zu nahezu gleichen mittleren Wärmeübergangskoeffizienten an allen Rippen der gesamten Anordnung führt. Veränderungen an der Austrittsgeometrie beeinflußten nur die weniger dicht gepackten Anordnungen und auch hier nur die äußerste Rippenreihe.

ВЛИЯНИЕ ГЕОМЕТРИЙ ВХОДА, ВЫХОДА И РЕБРА НА ИГОЛЬЧАТЫЕ РЕБРА, ОБТЕКАЕМЫЕ ПОТОКОМ С ПОВОРОТОМ

Аннотация—Проведено исследование пучка цилиндрических игольчатых ребер в случае, когда поток воздуха, поступающий в пучок со стороны плоскости концов ребер, совершает поворот при прохождении через пучок и выходит из него в поперечном направлении. Коэффициенты теплопереноса для каждого ребра и суммарные перепады давления определялись экспериментально. Сформулирована расчетная модель для определения интенсивности теплопереноса в пучке с учетом того факта, что не все ребра в пучке омываются потоком воздуха с одинаковой скоростью. На основе модели проводилось сравнение интенсивности теплопереноса в различных пучках при той же скорости подачи воздуха и той же разности температур между пластиной основания и воздуха на входе. Особое внимание обращено на исследование влияния различных геометрий входа и выхода, а также на плотность упаковки ребер. Показано, что частичное экранирование входа позволяет получить почти одинаковые коэффициенты теплопереноса для каждого ребра в пучке. Геометрия выхода оказывает влияние на коэффициенты теплопереноса только в случае менее плотно упакованных пучков и то только в самом крайнем ряду.